Optical Communications Performance with Realistic Weather and Automated Repeat Query

Loren Clare,* Gregory Miles,* and Julian Breidenthal*

ABSTRACT. — Deep-space optical communications are subject to outages arising from deterministic clear line-of-sight dynamics as well as unpredictable weather effects at the ground station. These effects can be mitigated using buffering and automatic retransmission techniques. We provide an analysis that incorporates a realistic weather model based on a two-state Markov chain. Performance for a hypothetical Mars 2022 optical mission is derived incorporating dynamics over an entire 728-day synodic cycle, during which link passes and link data rate vary. Buffer sizing is addressed and operational implications are identified. Also, buffer occupancy results are extended for deep-space missions spanning a range of link data rates.

I. Introduction

Substantial advancements have been made toward the use of optical communications for deep-space exploration missions, promising a much higher volume of data to be communicated in comparison with present-day RF-based systems. However, the optical link is subject to outages from time to time caused by weather effects at the ground station(s), in addition to predictable outages arising from geometric visibility. To mitigate these outages, an automatic repeat query (ARQ) retransmission method can be used, supported by a reverse channel for acknowledgment traffic.

An ARQ system for deep-space communication functions as follows. Data to be transmitted are organized into packets, and the sender maintains both an active queue of packets awaiting transmission, and a pending queue of packets that have been transmitted but not acknowledged as successfully received. These two queues together constitute the sender's data buffer.

Whenever the link is active, and there are packets in the active queue, the sender transmits packets and simultaneously moves them to the pending queue in case they need to be retransmitted later. When the packet is successfully received by the receiver, the receiver transmits an acknowledgement message back to the sender on a reverse channel. The

* Communications Architectures and Research Section.

The research described in this publication was carried out by the Jet Propulsion Laboratory, California Institute of Technology, under a contract with the National Aeronautics and Space Administration.

sender then removes the successful packet from the pending queue. A reliable reverse channel for the acknowledgment messages is helpful to system efficiency and performance.

If the sender receives no acknowledgment for a transmitted packet within a chosen duration, the sender returns the packet in the pending queue back to the active queue for another retransmission attempt. Typically, the chosen duration is the round-trip transmission time, plus an allowance for processing delays. If the link has an outage scheduled within the chosen duration, the chosen duration is increased to account for delays engendered by the wait for the link to become available again, to avoid retransmission attempts that are certain to be fruitless. Typically, the packet returning to the active queue is placed at the front of the queue to minimize latency variation.

The ARQ system has the property of providing a nearly complete set of data packets at the receiver, provided that the offered load at the sender's active queue is balanced with the link capacity, subject to constraints on latency. We say nearly complete because data can be "lost" or discarded if queues overflow.

We examined the performance of such a system under the assumption that the link is unreliable when it is scheduled to be available, and in one of two states: either functioning correctly (Good), or not functioning at all (Bad). We further assumed that transitions between the two states happen at random times, with constant probabilities per unit time of transition between the two states: p_{GB} for the probability per unit time of going from a Good to a Bad state, and p_{BG} for the probability per unit time of going from a Bad to Good state. This is a Gilbert–Elliott Markov chain model, which possesses mean sojourn times $E(G) = 1/p_{GB}$ for the Good state and $E(B) = 1/p_{BG}$ for the Bad state. The equilibrium proportions of time spent in each state are constant in this model, with the values

$\pi_G = E(G) / [E(G) + E(B)]$ for the Good state, and

$\pi_B = E(B) / [E(G) + E(B)]$ for the Bad state.

We also assumed that the reverse channel is prompt and reliable.

The analysis we report here is a single-site analysis. This is an important case because ground segment development is expensive, making it likely that ground stations will be brought on line one at a time. At first, only a single station will be available, raising the question of what performance can be achieved with that single station given realistic weather. Our work is directly applicable to this situation, corresponding to early demonstrations of operational optical communication, and would also be applicable if the first few stations are dispersed around Earth, with more or less only a single station in view at any given time.

Our ARQ analysis can be directly extended to the case of multiple stations, with only a single station in view at any given time, simply by adjusting the visibility schedule. Our analysis does not fully treat situations where multiple sites are in view simultaneously but residing in uncorrelated or quasi-correlated weather conditions, which is the so called "site

diversity" approach. Some prior reports discuss such networks but without ARQ; addition of ARQ to such analyses remains as future work. However, our single-station analysis provides an important foundation for that work.

In Section II, we derive realistic values for the model parameters based on historical weather data for two sites near to Goldstone, California, which is under consideration as a potential optical ground station site. Discussion of the quality of the model's fit to empirical data is provided.

The performance of the ARQ system is provided in Section III. We evaluated the key metrics of data loss rate and latency using a queueing theoretical approach and a discrete-event simulation that incorporated the Gilbert–Elliott weather model. Details of this analysis under assumptions of statistical stationarity are provided in [1], and summarized below. This analysis provides the means to determine what spacecraft buffer size provides sufficient overflow loss performance for an optical channel capable of a given data rate.

These deep-space optical link ARQ results are extended in Section IV to characterize the system performance for a Mars 2022 mission scenario in which the daily channel capacity varies significantly over the 728-day synodic period. The achievable data rate ranges 2 orders of magnitude over this interval, and in addition, the daily pass duration varies more than a factor of 2 [2]. This causes a very large difference in potential volume of data per day that may be returned over the course of the synodic period. We therefore propose a method for selecting the buffer capacity, as well as a time-dependent operational limit on offered traffic load, so that excellent performance extends over the duration of the overall mission. Throughput and loss performance is presented as a function of time within the synodic period based on the proposed mission operations approach.

However, a Mars mission is not the only potential application of optical communications; optical communications offers great promise to a wide range of deep-space missions. As identified in [3], these missions vary both regarding the capability of the optical terminal (including small, medium, or large aperture) as well as the distance of the link between Earth ground station and spacecraft. We consider general ARQ performance across a wide range of missions in Sections V and VI. First, we show that the one-way light time (OWLT) (the distance divided by the speed of light) considered in isolation has a relatively small impact on ARQ performance. This allows us to extend results to a wide range of missions having different optical link data rates without regarding OWLT. We derive the mean and 95th-percentile statistics for the number of packets in the buffer, assuming an infinite buffer capacity. These enable estimation for the buffer capacity required to achieve acceptable performance; generally, we have found that use of the 95th-percentile value results in about 1 percent data loss.

Section VII provides a summary of the results of our analysis.

II. Weather Effects

A. Weather Parameters

Earth's atmosphere has three characteristics that are significant to optical communications systems: atmospheric attenuation including both absorption and scattering loss, sky radiance, and turbulence. All of these are time-varying quantities, partly predictable and partly unpredictable in a deterministic sense. The predictable aspect arises due to constantly changing relative orientation between the spacecraft, the Earth station, the orientation of the Earth station horizon (or equivalently, its zenith), and the Sun. The unpredictable aspect arises due to fluctuations of atmospheric characteristics on a range of time scales ranging from minutes to decades. Although some predictions can be made concerning atmospheric characteristics, the predictions are inherently statistical in nature.

Xie et al. analyzed the predictable time-varying aspect using the Strategic Optical Link Tool (SOLT) program as described in [2]. Their assumptions correspond closely to the "cloud-free line of sight (CFLOS)" condition used by a number of authors to compile statistics on viewing conditions at potential sites for Earth optical stations. We took [2] as our reference for link performance in the Good state of the Gilbert–Elliott model.

For the unpredictable time-varying aspect, we assumed that when conditions are worse than assumed by [2], that is, under nonclear, higher-than-desert-daytime turbulence, or high wind conditions, degradation of the optical system is so great that the link is blocked. This is realistic for deep-space links, where link parameters will probably be sequenced well in advance of use, and there is an overall goal of maximizing data return. In principle, it is possible to close the link in worse-than-clear conditions, e.g., thin clouds or haze, by adjusting the data rate and modulation order; however, this would require either fast adaptation to short-term changes on the ground, or policies to design links to function continuously at lower data rates. The overall data return from a continuously lower strategy, however, is so much less than permitted by CFLOS conditions that to do so would strongly contradict the goal of maximizing cumulative data return. Neither the fast adaptation or the continuously lower strategies are planned at present, though fast adaptation might eventually be possible. If it does become possible, our assumption of complete loss during slightly cloudy times is pessimistic. We do not have a careful evaluation of the degree of pessimism at this time, but Table 5 of [5] suggests that an additional 10 to 15 percent of time might be usable at Table Mountain, if one allows for 1 to 2 dB attenuation and the corresponding increase in sky radiance.

B. Historical Weather Data — Fraction of Time with Cloud-Free Line of Sight

We equated the fraction of time when there is a cloud-free line of sight with the availability of the optical link in the Good state. For historical information on cloud-free line of sight, we referred to the data sets on single-station CFLOS described by Wojcik et al.[1]; also see [4–8], which are summarized in Table 1.

[1] G. S. Wojcik, H. L. Szymczak, R. J. Alliss, and M. L. Mason, *JPL CFLOS Project Fiscal Year 2004–05 Final Report* (internal document), Jet Propulsion Laboratory, Pasadena, California, September 7, 2005.

Table 1. Historical average cloud cover at selected sites.*

Reference (Source)	[7]	[4]	[6]	†	[5]
Base of observation	Ground, trained human	Ground, trained human	Ground, trained human	Satellite, camera	Ground, camera
Statistic	Average Clear Sky Time (CFLOS est.)	Average Clear Sky Time	Average Clear Sky Time (CFLOS est.)	Average CFLOS	Average Clear Sky
Time period	1973–1999	1991–1993, 1997–1999	1992–1995, 1997–1998	2003-2004	2008–2010
Location					
Las Campanas, Chile	—	—	—	82%	—
La Silla, Chile	—	—	—	81%	—
Gamsberg Table Mtn, Namibia	—	—	—	75%	—
Mauna Kea, HI	—	—	—	69%	—
Goldstone DSN, CA	—	—	—	66%	—
Daggett, CA	51% (67%)	41%	—	—	—
Kitt Peak, AZ	—	—	—	61%	—
Tucson, AZ	44% (61%)	50%	—	—	—
Haleakala, HI	—	—	—	61%	—
Palomar, CA	—	—	—	60%	—
Table Mtn, CA	—	—	—	60%	69%
Edwards AFB, CA	29% (62%)	27%	25% (62%)	—	—
White Sands, NM	—	—	—	54%	—
El Paso, TX	40% (60%)	45%	—	—	—
Starfire Optical, NM	—	—	—	52%	—
Albuquerque, NM	34% (54%)	33%	—	—	—
Canberra DSN, Australia	—	—	—	48%	—
Madrid DSN, Spain	—	—	—	45%	—

† Wojcik et al., September 7, 2005, op cit.

* The table columns are ordered by date of observation, and the table rows are ordered by average CFLOS as reported by Wojcik et al. In cases where two nearby sites were reported in different studies, the sites are associated in a single table row. Values in parentheses reflect an estimated CFLOS computed by adding 75% of the Average Scattered Sky fraction to the Average Clear Sky fraction.

It is important to recognize that there was substantial month-to-month and year-to-year variation in the observed data. For example, in [7], the annual average clear sky at Edwards Air Force Base varied from 12 percent to 55 percent with a standard deviation of 9 percent about the 29 percent average over all years included in the study. Also in [7], the monthly average, averaged over all years, of clear sky at Edwards ranged from 11 percent to 49 percent. We are aware of anecdotal reports of changes in sky conditions associated with weather cycles such as El Niño, recent drought conditions in California, and possibly long-term climate change. Therefore, operational link planners should consider the possibility that the actual weather experienced by a particular future mission may be different than historical averages.

As much of the early discussion focused on clear-sky conditions, we have represented that information here for comparison purposes, but clear sky is a more severe constraint on the weather than is CFLOS. That is, under scattered clouds there is still some area of the sky that is cloud free that would add to the fraction of time that could be useful for optical communications. As a result, all the clear-sky fractions reported are substantially lower than CFLOS for the same or nearby locations. Accounting for this bias is problematic, because the coarse bins used for human observations in the relevant studies obscure detailed information as to the proportion of sky that is open. However, we have indicated an approximate value in Table 1 that increases the clear sky fraction by 75 percent of the time that scattered cloud conditions were observed. The choice of 75 percent for the credit factor is derived from the average of the endpoints of cloud coverage, for the conditions reported as "scattered" (0<cloud coverage<4/8 of the celestial dome). The 75 percent value turns out to yield results extremely close to the CFLOS reported in some of the references using completely different methods, for the same or similar sites. However, the value in principle suffers from the same problem the underlying data record has regarding obscuration of detailed observational information about fraction of the sky that was actually covered.

We adopted 67 percent as the average Goldstone CFLOS, which is supported directly by [7] and Wojcik et al.,[2] and indirectly by all of the weather references as listed in Table 1. We adopted the likely range of annual variation of CFLOS between the worst year observed (1984) and best year observed (1973) as 38 percent to 72 percent. This range relies on the adjusted CFLOS described in the preceding paragraph, applied to [7]. Another useful reference point is that the best available sites on Earth have CFLOS around 80 percent.

C. Historical Weather Data — Duration of Clear Sky

Besides the aggregated fraction of time with a cloud-free line of sight, the temporal aspect is also an important aspect of the optical channel. Two data sets, [5] and [6], provide statistics on duration of clear-sky periods: Amini et al. [6] analyzed the durations of visually determined clear-sky conditions at Edwards Air Force Base, California, for the seven-year period 1992 through 1998, and Nugent et al. [5] derived the durations of clear sky at Table Mountain, California, using an infrared imager, for the two years July 15, 2008, to July 14, 2010.

---

[2] Wojcik et al., September 7, 2005, op cit.

In Section II.D, we will apply a Gilbert–Elliott channel model. This model possesses a probability density function for the duration of clear sky that is a geometric distribution of the form $p_{GB} * (1 - p_{GB}) ^T$, where T is the discrete duration of clear sky and p_{GB} is as described in the introduction. We fit this distribution to the statistics of hourly cloud cover estimates reported in [6], for long-term average, annual averages, and average by month. The long-term average fit appears in Figure 1, where it can be seen that the assumed distribution conforms very well to the observed data for durations greater than 2 hours. For zero duration, in all cases reported in [6], the probability of zero duration was zero, consistent with their data acquisition practice. Furthermore, in nearly all subsets of the data in [6], the probability of 1-hr duration was significantly elevated compared to the geometric distribution, which we believe indicates that the channel process is correlated, not random, below durations of about 2 hours. That is, if it is clear now, it is somewhat more likely to remain clear for an hour or so than one predicts based on the assumption of constant transition probability. For this reason, the fit we report here was fit to durations of 2 hours and greater.

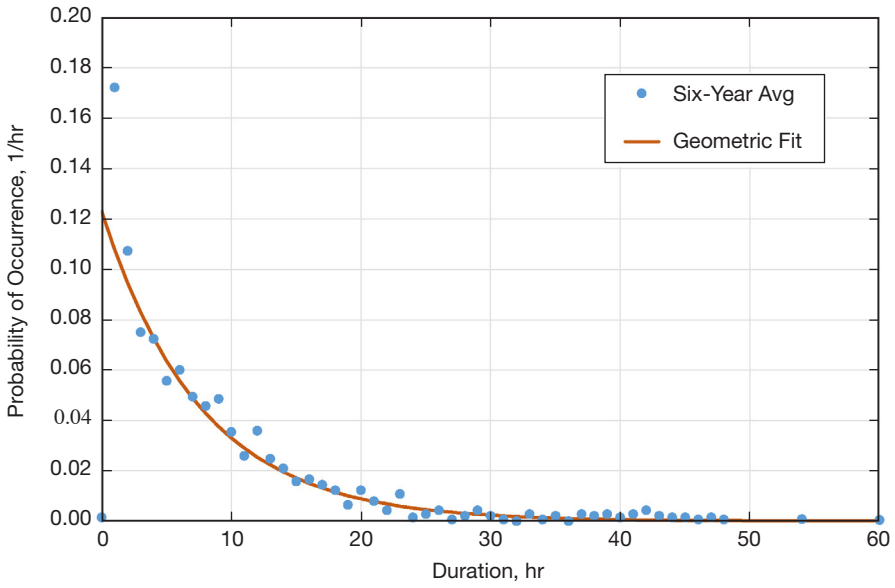

Figure 1. Observed durations of clear sky, six-year average from [6], with fitted geometric distribution, p_{GB} = 0.123014 (1/hr).

The statistics reported in [6] show substantial variation by year and by month, reflecting the chaotic and possibly nonstationary nature of weather. We detailed the range of variation in Table 2. Lacking information on time spent in cloudy conditions from the reference, we estimated in Table 2 the Bad-to-Good transition probability from an identity associated with our model,

$$(p_{GB}/p_{BG}) (\pi_G/\pi_B) = 1$$

using the equilibrium proportion of time spent in each state (π_G = 0.62 and π_B = 0.38), consistent with the Edwards Air Force Base CFLOS fraction in Table 1.

Table 2. Summary statistics of clear sky durations, Edwards Air Force Base, 1992–1998.*

Statistic	Probability of Clear-to-Cloudy Transition p_{GB} (1/hr)	Corresponding Mean Sojourn Time Clear $1/p_{GB}$ (hr)	Probability of Cloudy-to-Clear Transition p_{BG} (1/hr)	Corresponding Mean Sojourn Time Cloudy $1/p_{BG}$ (hr)	Notes
Month with shortest average duration	0.3258	3.1	0.5315	1.9	1994 October
Year with shortest average duration	0.1486	6.7	0.2424	4.1	1997
Average of all years	0.1230	8.1	0.2007	5.0	1992–1998
Year with longest average duration	0.0906	11.0	0.1478	6.8	1995
Month with longest average duration	0.0281	35.6	0.0459	21.8	1995 October

* Assuming equilibrium fractions Good $\pi_G = 0.62$ and Bad $\pi_B = 0.38$.

We also fit a geometric distribution to the statistics of 10-min cloud cover estimates reported by [5], as shown in Figure 2.

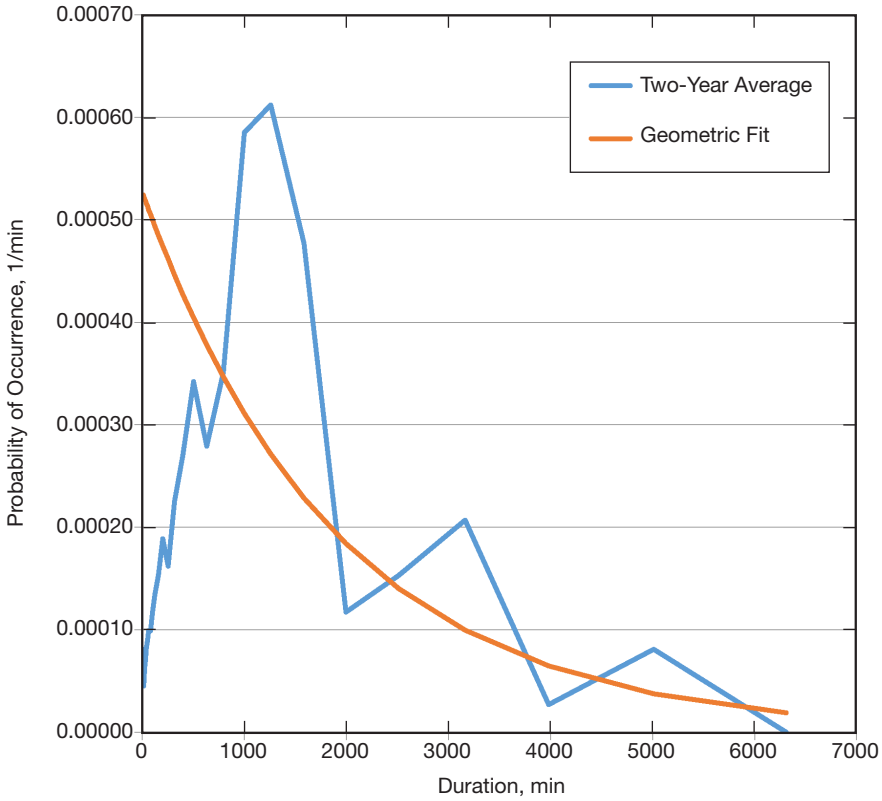

Figure 2. Observed durations of clear sky, two-year average from [5], with fitted geometric distribution, $p_{GB} = 0.0005270$ (1/min).

D. Weather Model

We assumed a 2-state Gilbert–Elliott Markov Chain model in which the channel moves between Good (clear sky) and Bad (cloudy) states at random times according to constant transition probabilities as described in the introduction. A discrete-time model is assumed, so that the sojourn time within the weather state G or B is geometrically distributed with parameter p_{GB} and p_{BG}, respectively. We also use the mean sojourn times in each state, and the equilibrium proportion of time spent in each weather state, as described in the introduction since they are easier to relate to empirical effects.

Although short-term packet transmission failure errors can occur during Good weather, for simplicity we assume zero probability of link errors in the G state. Also, successful transmissions might occur during the Bad weather state; however, for simplicity we assume all downlink transmissions fail while in the B weather state. These simplifying assumptions imply that the probability of a successful transmission when the link is active is simply π_G. One may generalize our weather effects model to incorporate many possible weather states, with a corresponding transmission success probability associated with each weather state. We believe the current model is sufficient to capture key system factors, and leave this generalization for future work.

Figure 3 (from [1]) depicts the qualitative differences in potential link behavior that might result from several different 2-state weather models based on different parameter selections. These vary both in terms of the ratio of time spent in the Good versus Bad state (1:1 or 2:1) and with regard to duration in a given state (the bottom two examples behaving 4 times slower than the top two on average).

III. Analysis of Automatic Repeat Request

A. Weather Model Incorporation into ARQ Queueing Model

A method to evaluate the performance of an ARQ system as applied to a deep-space optical link was given in [1]. The model includes effects from both short-term and long-term system influences. It was found that ARQ performance is dominated by long-term dynamics arising from weather conditions that persist for hours. Short-term effects, such as link drop-outs on the order of seconds due to space platform pointing errors, were found to lower throughput but have very little impact on key ARQ system engineering parameters, in particular, on spacecraft buffer sizing and data loss from buffer overflow. Deep-space optical link ARQ performance is therefore crucially dependent on accurate consideration of the weather model. The method of fitting evidence-based weather parameter values to the weather model used in conjunction with ARQ analysis was presented in Section II.C.

B. ARQ Analysis

Performance of a deep-space optical link using ARQ was derived [1] using a queueing model approach and discrete-event simulation. New traffic is modeled as a deterministic and constant arrival process of fixed-length data packets at the spacecraft. Downlink transmis-

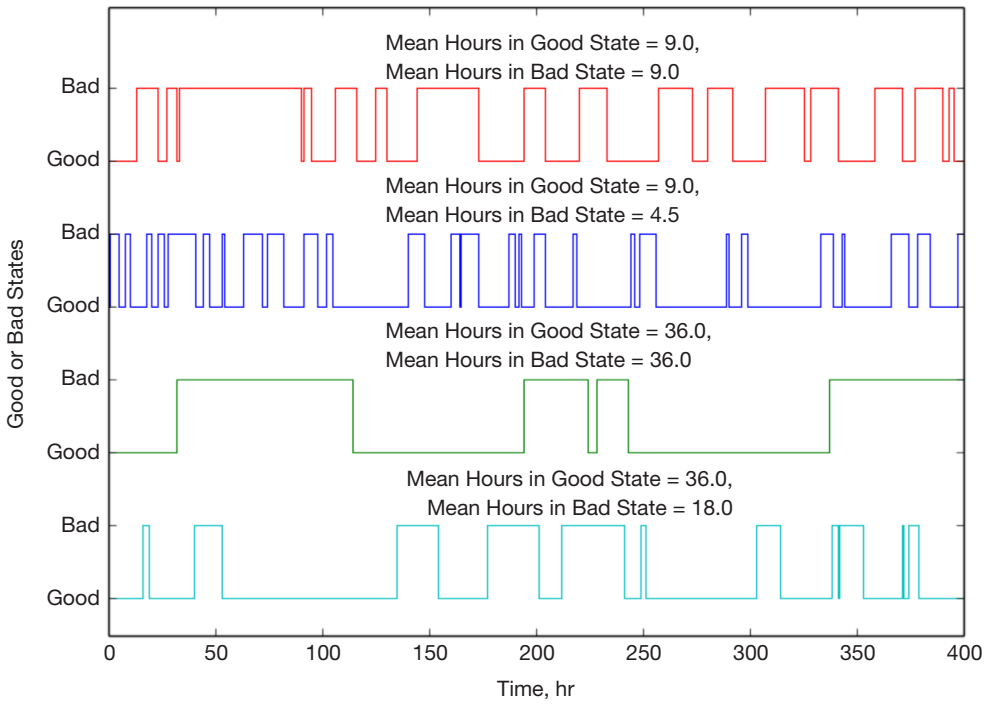

Figure 3. Example parametric weather model realizations.

sions to the Earth ground station are scheduled; in Section IV we will assume the link is active whenever geometry avails it. Packets are placed in a buffer to wait for a transmission opportunity. The buffer has finite capacity, so packets are lost when it overflows. An uplink is used for error-free acknowledgment during the ground station passes. Packets remain in the buffer until acknowledged. Unsuccessful packet transmissions are detected after a scheduled interval, whereupon the packet remains in the buffer for retransmission. Only buffer overflow packets are lost.

Selective repeat (SR) continuous ARQ is assumed, as simpler ARQ variants will suffer substantial performance degradation with the very high "delay-bandwidth product" environment of deep-space communications. SR ARQ efficiently transmits each successful packet once provided ACKs are reliable. Specifically, we assume the Licklider Transmission Protocol (LTP) of the disruption-tolerant networking (DTN) suite [8] that is well-suited to deep-space communications. In particular, the ARQ process is aware of the link schedule and correspondingly adjusts timeout timers, which provides some gain in efficiency.

The set of inputs to the ARQ analysis includes:

- Link schedule; pass duration per day
- Burst transmission data rate r_T
- Data packet arrival rate r_A
- Buffer capacity
- Weather model parameters {E(G), E(B)} where E(G)=mean duration of continuous Good weather and E(B)=mean duration of continuous Bad weather

- One-way light time
- Duration of simulated time (complete run)

The primary set of outputs of the ARQ analysis are:

- Throughput
- Loss rate due to buffer overflow r_L
- Latency statistics
- Queue-size statistics

The offered load is the packet arrival rate normalized by the long-term system capacity. As is typical of general queueing systems, congestion quickly rises as the offered load approaches 100 percent. In [1], the offered load was constant; we consider dynamic offered load in Section IV, taking into effect the time-dependent channel capacity. The latency is the time from when the packet first arrives to the spacecraft until it is successfully received on the ground (conditioned on not having been lost due to buffer overflow). The queue-size is how many packets occupy the buffer.

A general trend revealed in [1] was greater congestion arose with larger "weather cycles," where a cycle is the time to next reenter a weather state (G+B). Thus, selection of larger E(G)+E(B) will tend to place greater demand on buffer resources. Figure 4 presents the mean queue size versus the mean weather cycle duration. Included are the cases {E(G)=30.6, E(B)=40.9} and {E(G)=8.1, E(B)=5.0}, which correspond to a fit of empirical data collected for the Table Mountain Facility (TMF) and for Edwards Air Force Base (EAFB) respectively, as shown in Section II.C.

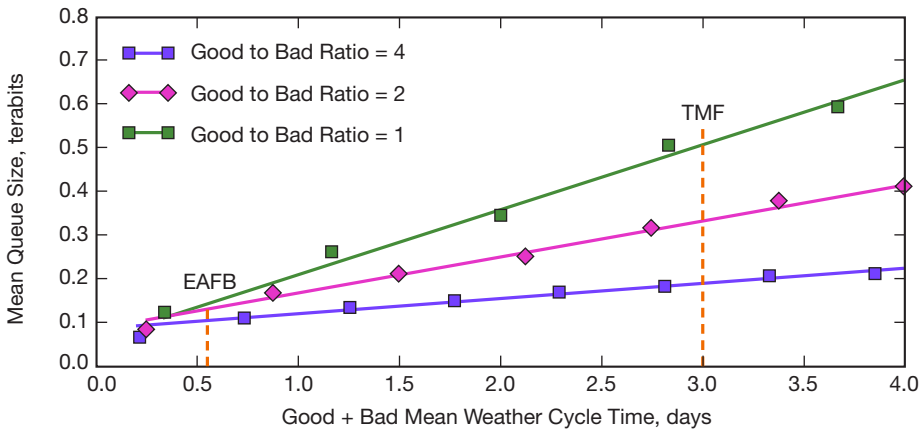

Figure 4. Packet loss rate vs. offered load, Good and Bad weather. Mean duration = 9.5 hr, r_T=10Mb/s.

An example result from [1] is loss rate performance across a range of offered load values. The same or lower loss rate can be achieved with a smaller buffer capacity at the cost of operating at a reduced offered load. Figure 5 presents the packet loss rate as a function of the offered load as it ranges between 25 percent to 95 percent of channel capacity when the weather is defined by mean Good and Bad durations of 9.5 hr each.

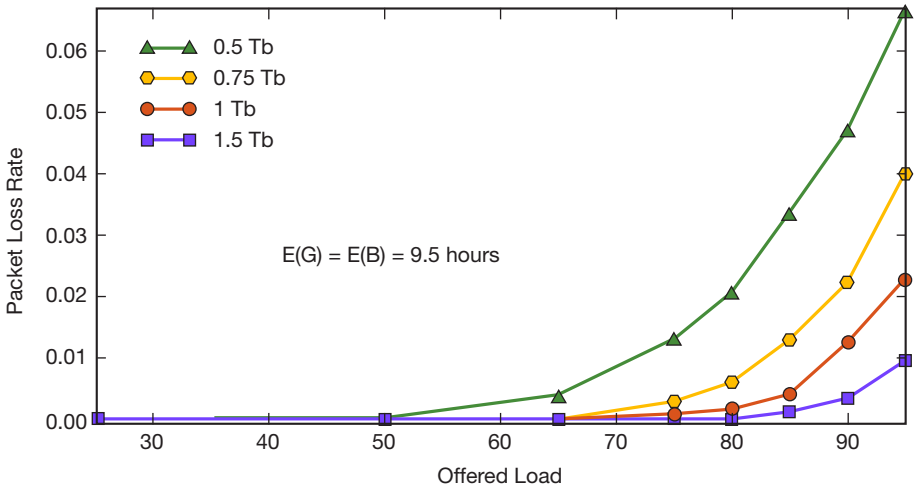

Figure 5. Packet loss rate vs. offered load, Good and Bad weather. Mean duration = 9.5 hr, r_T=10Mb/s.

As another example, Figure 6 provides both the mean queue-size and the mean latency versus offered load capacity for two different weather conditions {E(G), E(B)}={9.5, 9.5} or {36, 36} and an infinite buffer capacity. The 95th-percentile queue-sizes were found to be approximately 3 times the mean values (not shown below).

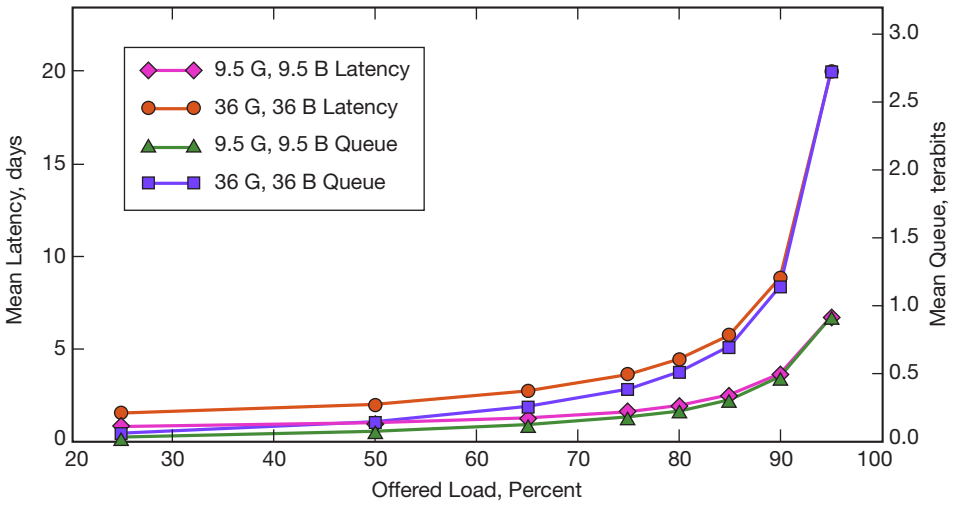

Figure 6. Mean latency and mean queue-size vs. offered load, r_T=10Mb/s.

IV. Mars 2022 Mission Performance

We consider the operation of a Mars mission in the 2022 time frame. The Earth–Mars relative geometry varies over a 728-day synodic period, yielding a correspondingly varying achievable daily burst transmission rate capacity that is presented in [2] for a medium-aperture space terminal (22 cm, 4 W) and three possible ground apertures: 11.8 m, 8 m, and 4 m. It is found that the optical link burst transmission rate varies over 2 orders of magnitude during this cycle. The channel pass capacity is the burst transmission rate times the availability determined by the weather condition. We conservatively assume the weather is parameterized as E(G)=E(B)=9.5 hr, so that the channel availability is 0.5.

We assume a single optical ground station is used to support the Mars 2022 spacecraft.

In addition to the achievable link data rate varying over the synodic period as the Mars–Earth distance changes (between about 0.5 AU to 2.7 AU), the daily pass duration will vary (between about 5.17 hr and 11.0 hr) according to the geometric line-of-sight dynamics. Channel capacity C(t) is determined by the combination of the achievable link data rate and the pass duration as they vary over the synodic period. Ambient ground station weather patterns may slowly vary over the seasons; however, we assume constant weather parameters for simplicity.

Generally, it would be desirable to set the offered traffic rate $r_A=r_A(t)$ as a fixed proportion of the channel capacity C(t), setting the offered load at say $r_A(t)/C(t)=80\%$ for reasonably high channel utilization. We also wish to bound the overflow loss rate at, e.g., $r_L=1\%$ over the entire period. However, satisfying this loss requirement at the peak channel capacity over the 728-day period will require a very large buffer capacity. A compromise is suggested, in which one chooses the buffer capacity to satisfy $r_L=1\%$ loss at 80 percent load at a threshold capacity. Suppose that one chooses this threshold as 33 percent of the maximum capacity. For example, for the 11.8-m ground aperture case, the maximum channel capacity is 99 Mb/s, so the threshold rate is 32.6 Mb/s. Using results from [1], the required buffer capacity is found to be 6.65 Tb. The mission operations concept is: Whenever the channel capacity <32.6 Mb/s, the offered traffic load is 80 percent of capacity. However, when the channel capacity >32.6 Mb/s, the offered load is lowered to that level such that the 1 percent loss rate is maintained. In this example, we found that at the peak channel capacity of 99 Mb/s, the offered load is 40 percent of capacity, or 40 Mb/s.

Figure 7 illustrates this situation for the three aperture sizes and E(G)=E(B)=9.5hr weather. The offered load is depicted for each case along with the channel capacities. Transition points where the offered load transitions between fixed and varying values are shown with ovals. The buffer capacities used are 6.65 Tb, 4.15 Tb, and 1.45 Tb for the 11.8-m, 8-m, and 4-m aperture cases, respectively.

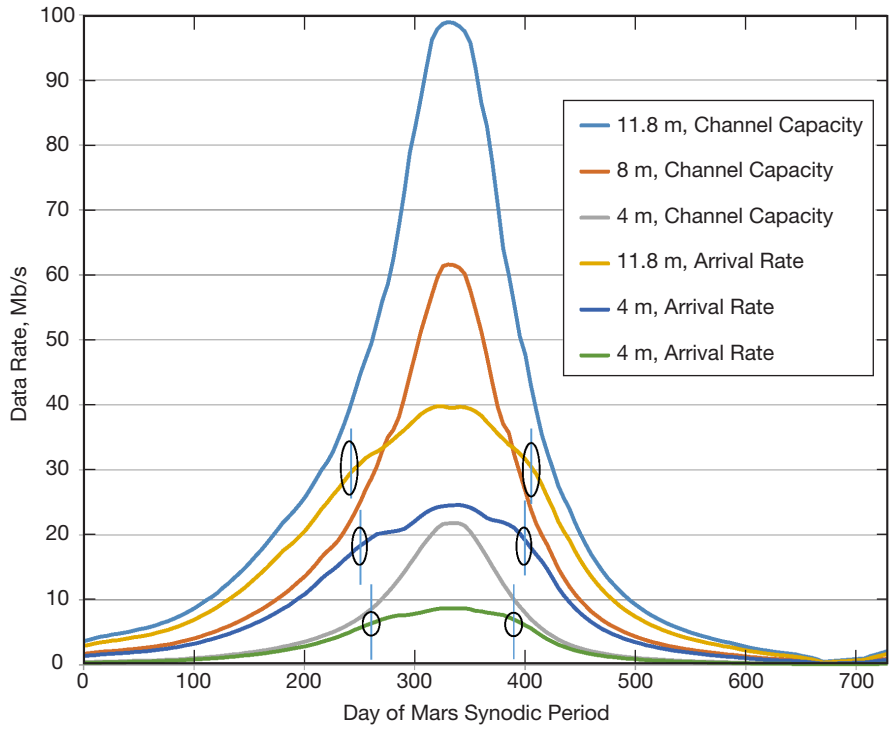

Figure 7. Channel capability and traffic arrival rates vs. time, three ground apertures.

The total capacity volume over the entire Mars synodic period is found to be 680 Tb, 384 Tb, and 122 Tb for the 11.8-m, 8-m, and 4-m apertures, respectively. This averages to 934 Gb/day, 527 Gb/day, and 168 Gb/day, respectively, over the 728-day Mars synodic period. The sizes of the chosen buffer capacities relative to the average daily capacity volumes are 7.1, 7.9, and 8.6, respectively.

Using the time-varying offered traffic profiles defined in Figure 7 and time-varying pass lengths, the total volumes of offered traffic over the entire Mars synodic period are 398 Tb, 226 Tb, and 72 Tb, respectively, and the average daily offered traffic is 545 Gb/day, 310 Gb/day, and 98 Gb/day, respectively. This corresponds to a long-term utilization (carried load to channel capacity ratio) of about 59 percent for all three optical ground apertures. For comparison, the X-band capacity over the Mars synodic period using the same pass times would be 6.46 Tb, corresponding to a daily average of 8.87 Gb. However, we assumed continuous (24/7) X-band coverage using existing Deep Space Network assets, in which case the X-band capacity volume over the Mars synodic period using the same pass times would be 17.4 Tb, corresponding to a daily average of 23.9 Gb. Thus, we found that if the spacecraft buffer is reduced to ~60 percent of the size it would have if sized for peak offered traffic, and the offered traffic reduced to maintain fixed loss rate, optical communications still offers 4 to 20 times the volume of X-band.

During the times when operating the optical link at 80 percent offered load, the latency performance remains statistically constant. When operating at lower offered loads, latency is lower as the channel becomes somewhat less utilized (as low as 40 percent utilization at the peak rate). Figure 8 presents the mean latency as a function of time for the same

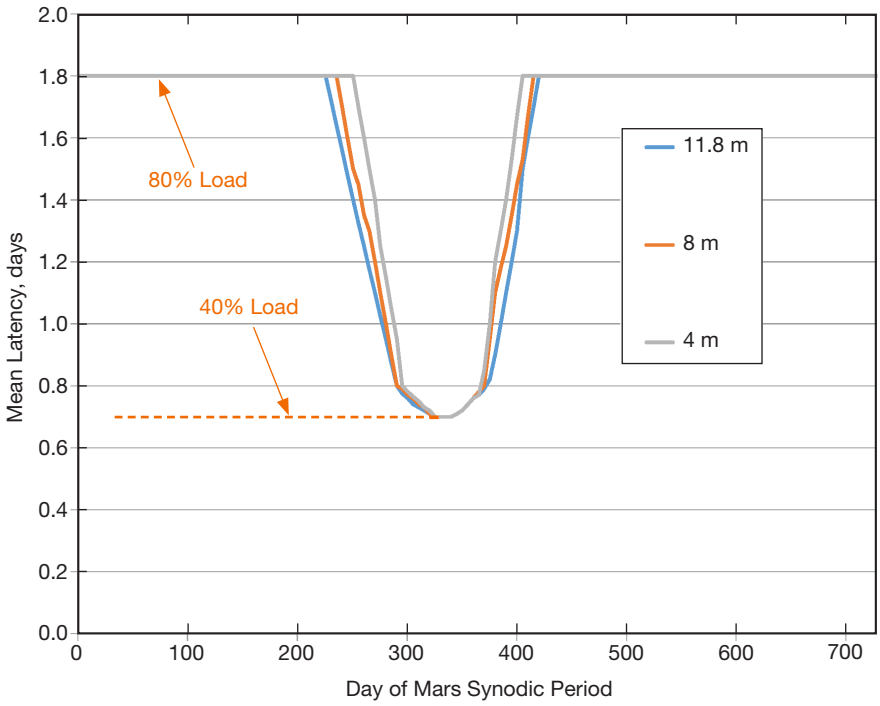

Figure 8. 95th-percentile latency vs. time, three ground aperture sizes.

E(G)=E(B)=9.5hr case and three ground station aperture choices. It is noted that mean latency ranges from 0.7 days at the peak data rate to 1.8 days during times when the load is 80 percent.

A loss rate performance of 1 percent of the offered traffic will be maintained using the operational approach described in the above example. Additional second-tier traffic may be "inserted" during those times when the system is not busy transmitting the primary traffic, provided the primary traffic maintains strict priority over resources. This may yield a reasonable amount of additional potential volume, such as when the primary offered traffic is near only 40 percent load. However, this second-tier "best effort" traffic will not enjoy the quality of service (QoS) of the primary traffic, with higher loss and latency performance expected.

V. One-Way Light Time Dependence

The following presents performance as a function of varying one-way light time (OWLT) propagation delay for the optical link. We fix the parameters r_T=10Mb/s, 80 percent offered load, and E(G)=E(B)=24hr, and then vary OWLT. Of course, if one were to vary the range (OWLT) to the spacecraft while holding its capabilities constant, r_T would also change; however, here we are focusing on the OWLT parameter only and hold all other parameters fixed. Figure 9 depicts the mean queue size and mean latency across OWLT values spanning most of the solar system. We found that while larger OWLT will cause larger performance values, the effect is relatively small.

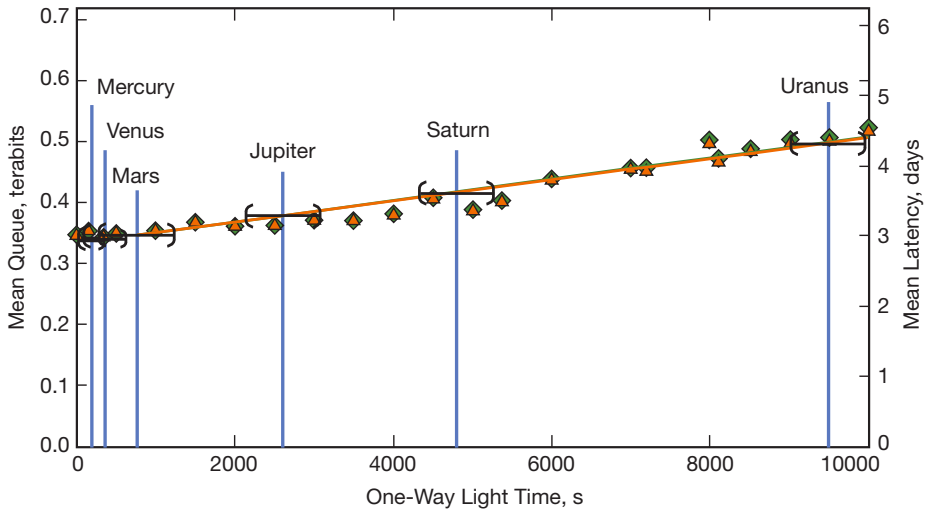

Figure 9. Performance impact of OWLT.

VI. Buffer Occupancy vs. Channel Capacity

A wide range of deep-space missions that may significantly benefit from the use of optical communications have been identified [3]. Results are derived for several deep-space mission scenarios selected to capture the realistic, driving values and span missions in the target time era. In all these scenarios, we focused on operation based on a single optical ground station. The key performance drivers are (1) proportion of time successful transmissions may occur, and (2) the burst transmission data rate. Another parameter that affects performance is the OWLT propagation delay; however, analyses indicate this has little overall impact (primarily influencing the size of the pending queue used for ARQ operation). Queue-size performance, which dictates buffer capacity sizing and overflow loss, is linearly (directly) dependent on the burst transmission rate, and summary results are presented below across the range of missions identified above in [3].

The performance is driven primarily by the portion of time transmissions may succeed, the offered traffic load, and the burst transmission data rate r_T. As was shown in Section V, the impact on performance of different propagation delays is relatively insignificant. Thus, once we derived performance for a particular offered load and r_T case, other missions' queue-size performance may be determined by simple scaling the burst transmission rate r_T. Given the offered load as a proportion of channel availability C, the loss rate and latency performance do not otherwise depend on r_T. In our analyses, we typically assumed that the offered load is 80 percent of the channel availability. Note that the weather impacts the ground terminal, and weather characterization applies equally across different mission spacecraft.

As an example, suppose the weather is modeled with mean Good duration E(G)=9.5 hr and mean Bad duration E(B)=9.5 hr. In our baseline r_T=10Mb/s example, we found that with an infinite capacity buffer and 80 percent offered load, the mean queue-size is 180 Gb and 95th-percentile queue-size is 550 Gb. We extrapolated to the set of missions identified in

[3] to determine their queue-size performances, shown in Figure 10 as the mean queue-size and the 95th-percentile queue-size. In this calculation, we ignored the variation in OWLT due to its relatively negligible effect. Choosing the 95th-percentile queue-size for the buffer capacity, then all missions will have the same loss rate of 1.73 percent (although the loss volume depends directly on the data arrival rate r_A). Also, all missions will have the same latency performance.

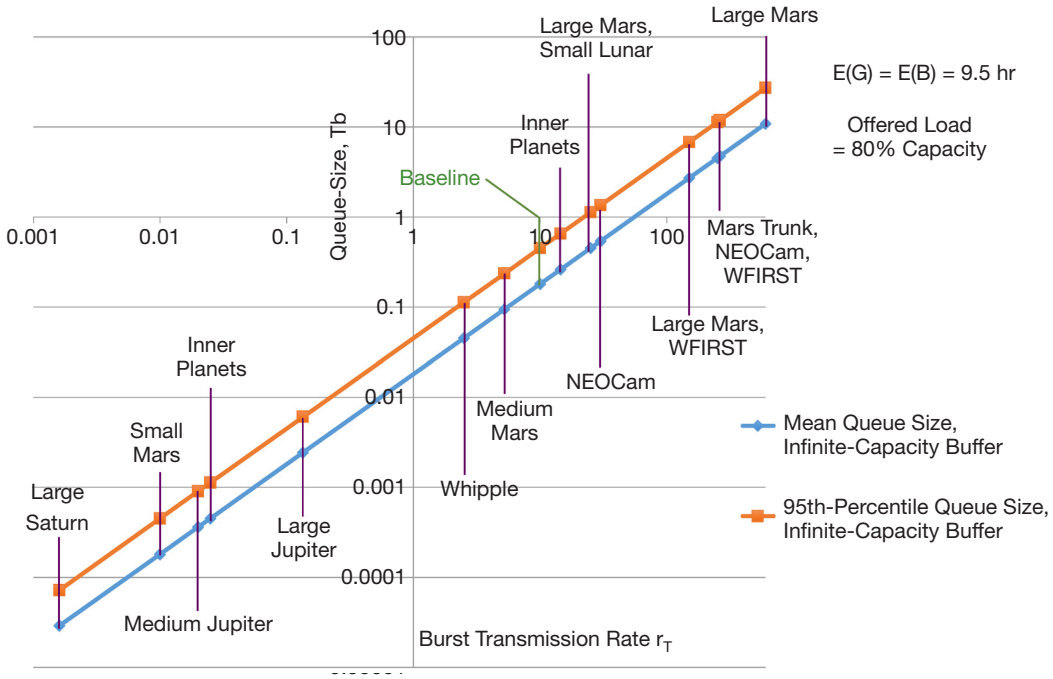

Figure 10. Queue-size performance vs. burst data transmission rate.

VII. Summary

We characterized weather conditions that impact deep-space optical communications, taking into account the histories of weather at relevant sites around the world. In our model of bad weather, a random process was assumed that could at any time make transitions between two states: a cloud-free state, and a cloudy state that completely interrupts data transmission. The weather process was characterized by mean fractions of time good and bad, and mean sojourn times in good or bad conditions. A range of values for these parameters was explored that encompasses the range of parameters observed in previous studies of weather conditions at several potential sites for an optical ground segment. Our analysis was a single-site analysis, which corresponds to the likely conditions of early operational demonstrations, and can be directly extended to the case of multiple stations dispersed around Earth with only one station in view at a time. Application of ARQ together with site diversity to mitigate weather would require further analysis, which would be supported by our single-site analysis.

Unpredictable outages due to weather can be mitigated using an ARQ technique. Analyses have determined that ARQ system performance is highly sensitive to the weather behavior, including latency and probability of data loss due to buffer overflow.

We derived performance for a Mars 2022 mission scenario that incorporates slow time variation of key deep-space optical link characteristics that arise over a 728-day synodic period. Both the achievable data rate and pass durations vary significantly over this period. Implications on mission operations are addressed, and a "compromise" engineering solution approach is offered that achieves good throughput over the entire period while requiring less buffer capacity. The mission offered traffic is limited to 80 percent of achievable capacity except when the Mars–Earth distance is small and achievable data rate is high, when lower offered load is mandated for reliable traffic. However, "best-effort" traffic that does not have the reliability quality of service may be added using strict priority discipline.

In addition, extensions to deep-space optical link ARQ performance analysis were presented that consider general performance over wide range of missions and associated optical data rates. It was shown that the isolated effect of the OWLT delay is relatively small on ARQ system performance, where here we ignore effects of distance on achievable link data rate. This result allows us to extrapolate buffer occupancy results, and therefore buffer sizing estimates, over mission spanning a wide range of required optical link data rates.

References

[1] L. Clare and G. Miles, "Deep Space Optical Link ARQ Performance Analysis," P*roceedings of 2016 IEEE Aerospace Conference*, Big Sky, Montana, March 5–12, 2016.

[2] H. Xie, D. Heckman, and J. Breidenthal, "Link Characterization for Deep-Space Optical Communications," *The Interplanetary Network Progress Report*, vol. 42-205, Jet Propulsion Laboratory, Pasadena, California, pp. 1–33, May 15, 2016. http://ipnpr.jpl.nasa.gov/progress_report/42-205/205D.pdf

[3] J. Breidenthal and D. Abraham, "Design Reference Missions for Deep-Space Optical Communication," *The Interplanetary Network Progress Report*, vol. 42-205, Jet Propulsion Laboratory, Pasadena, California, pp. 1–19, May 15, 2016. http://ipnpr.jpl.nasa.gov/progress_report/42-205/205B.pdf

[4] A. Biswas and S. Piazzolla, "The Atmospheric Channel," *Deep Space Optical Communications*, H. Hemmati, ed., Deep Space Communication and Navigation Series, Jet Propulsion Laboratory, Pasadena, California, October 2005.

[5] P. W. Nugent, J. A. Shaw, and S. Piazzolla, "Infrared Cloud Imager Development for Atmospheric Optical Communication Characterization, and Measurements at the JPL Table Mountain Facility," *The Interplanetary Network Progress Report*, vol. 42-192, Jet Propulsion Laboratory, Pasadena, California, pp. 1–31, February 15, 2013. http://ipnpr.jpl.nasa.gov/progress_report/42-192/192C.pdf

[6] P. E. Amini, S. D. Slobin, and S. Piazzolla, *Cloud Coverage Statistics for Optical Communications at Table Mountain Observatory, California, Based Upon 1992–1998 Surface Weather Observations From Edwards Air Force Base, CA*, JPL Publication 00-12, Jet Propulsion Laboratory, Pasadena, California, November 30, 2000.

[7] S. Piazzolla, S. D. Slobin, and P. E. Amini, *Cloud Coverage Diversity Statistics for Optical Communications in the Southwestern United States*, JPL Publication 00-13, Jet Propulsion Laboratory, Pasadena, California, November 30, 2000.

[8] M. Ramadas, S. Burleigh, and S. Farrell, S., Licklider Transmission Protocol, Specification, RFC 5326, Internet Engineering Task Force, Reston, Virginia: ISOC, September 2008.
https://tools.ietf.org/